Supplementary Information

Structure elucidation and construction of isomerisation pathways in small to moderate-sized (6 — 27) MgO nanoclusters: An Adaptive Mutation Simulated Annealing based analysis with quantum chemical calculations

Kuntal Ghosh*, Rahul Sharma†, Pinaki Chaudhury ‡

Adaptive Mutation Simulated Annealing (ASA)	**Simulated Annealing** (SA)
(i) Much higher chances of obtaining the global minimum in one single run	(i) Lower chances of obtaining the global minimum in one single run
(ii) Global minimum reached in lesser no of temperature steps (1)	(ii) Minima (local or global) reached in more no of temperature steps (1)
(iii) The optimisation parameters are automatically updated (hence, adaptive)	(iii) The optimisation parameters must be manually updated (if updated at all)

Table 1: Comparison of ASA and SA algorithms

*Department of Chemistry, St. Xavier's College, 30 Mother Teresa Sarani. Kolkata - 700016, India, email: kuntalghoshchem@gmail.com, Present Address: Department of Chemistry, Indian Institute of Technology Kanpur, Kanpur - 208016, India

†ORCID: 0000-0003-2999-1285, email: sharmamonty@gmail.com: Corresponding author, Department of Chemistry, St. Xavier's College, 30 Mother Teresa Sarani. Kolkata - 700016, India

‡ORCID: 0000-0002-5192-7338, email: pinakc@rediffmail.com: Corresponding author, Department of Chemistry, University of Calcutta, Kolkata - 700009, India

P_c	**Energy (in kJ/mol)**	**Gradient norm**	**First eigenvalue**	**Second eigenvalue**
0.0 (R)	-5795.6716	1.2511×10^{-9}	8.7912×10^{-4}	2.5349×10^{-3}
0.1021	-5795.5369	5.1269×10^{-7}	4.8667×10^{-4}	2.8009×10^{-3}
0.2042	-5795.2336	1.0665×10^{-6}	1.3886×10^{-5}	3.0061×10^{-3}
0.3063	-5794.9576	4.0469×10^{-7}	-5.9872×10^{-4}	2.7939×10^{-3}
0.3799 (TS)	-5794.8946	5.0278×10^{-10}	-1.1061×10^{-3}	2.5692×10^{-3}
0.5107	-5795.4000	6.1260×10^{-7}	-1.9736×10^{-3}	2.0788×10^{-3}
0.7148	-5799.1651	6.8466×10^{-6}	-2.3967×10^{-3}	1.7682×10^{-3}
0.9216	-5806.7956	7.3158×10^{-6}	3.5987×10^{-3}	4.1677×10^{-3}
0.9739	-5807.9061	8.9920×10^{-7}	3.5599×10^{-3}	4.1849×10^{-3}
1.0 (P)	-5807.9596	2.2071×10^{-7}	3.5637×10^{-3}	4.1435×10^{-3}

Table 2: Energy, gradient norm and first two eigenvalues of $(MgO)_8$ cluster at each P_c

P_c	**Energy (in kJ/mol)**	**Gradient norm**	**First eigenvalue**	**Second eigenvalue**
0.0 (R)	-6577.9406	1.0360×10^{-9}	1.5870×10^{-3}	1.5874×10^{-3}
0.1	-6577.2765	6.1838×10^{-6}	1.2559×10^{-3}	1.9551×10^{-3}
0.2	-6575.6834	1.1589×10^{-5}	8.0425×10^{-4}	2.2817×10^{-3}
0.3	-6573.3286	2.3571×10^{-5}	2.8989×10^{-4}	2.5225×10^{-3}
0.55	-6567.3134	1.3558×10^{-5}	-1.3569×10^{-3}	5.3591×10^{-4}
0.6495 (TS)	-6566.5729	6.3011×10^{-10}	-2.0892×10^{-3}	4.7841×10^{-5}
0.8	-6569.1573	7.6358×10^{-6}	-1.9831×10^{-3}	1.0565×10^{-3}
0.9	-6573.5535	1.6779×10^{-5}	9.5932×10^{-4}	3.1314×10^{-3}
1.0 (P)	-6576.3115	1.9702×10^{-6}	4.3135×10^{-3}	5.2629×10^{-3}

Table 3: Energy, gradient norm and first two eigenvalues of $(MgO)_9$ cluster at each P_c

P_c	**Energy (in kJ/mol)**	**Gradient norm**	**First eigenvalue**	**Second eigenvalue**
0.0 (R)	-8049.5664	1.7177×10^{-9}	1.1007×10^{-3}	1.7565×10^{-3}
0.1071	-8049.1677	6.9929×10^{-7}	1.0182×10^{-3}	1.7307×10^{-3}
0.2142	-8047.9812	5.7995×10^{-6}	8.2655×10^{-4}	1.6954×10^{-3}
0.3213	-8046.0958	1.4647×10^{-5}	4.9914×10^{-4}	1.6191×10^{-3}
0.4284	-8043.9179	2.5397×10^{-5}	-3.5674×10^{-5}	1.4876×10^{-3}
0.6977	-8040.0629	4.0953×10^{-6}	-1.4421×10^{-3}	9.6673×10^{-4}
0.7543 (TS)	-8039.8630	8.3168×10^{-9}	-1.5580×10^{-3}	9.1738×10^{-4}
0.8613	-8040.2347	1.8124×10^{-6}	-8.7926×10^{-4}	1.1763×10^{-3}
0.9712	-8041.2356	1.8483×10^{-6}	1.5488×10^{-3}	1.8425×10^{-3}
1.0 (P)	-8041.3757	1.7230×10^{-7}	1.6318×10^{-3}	2.5959×10^{-3}

Table 4: Energy, gradient norm and first two eigenvalues of $(MgO)_{11}$ cluster at each P_c

P_c	**Energy (in kJ/mol)**	**Gradient norm**	**First eigenvalue**	**Second eigenvalue**
0.0 (R)	-8843.1849	8.9789×10^{-12}	1.3134×10^{-3}	1.3142×10^{-3}
0.1	-8842.4170	8.8218×10^{-6}	1.0348×10^{-3}	1.6113×10^{-3}
0.2	-8840.4386	1.2585×10^{-5}	7.0335×10^{-4}	1.9131×10^{-3}
0.3	-8837.7605	9.2312×10^{-6}	2.5415×10^{-4}	1.5471×10^{-3}
0.45	-8833.1295	6.5741×10^{-6}	-7.9413×10^{-4}	4.2414×10^{-4}
0.5520 (TS)	-8831.5159	3.0247×10^{-7}	-1.6035×10^{-3}	1.2870×10^{-4}
0.75	-8835.6575	5.6468×10^{-6}	-5.5730×10^{-4}	2.8114×10^{-3}
0.8	-8836.4228	1.8454×10^{-5}	-1.3066×10^{-3}	2.6651×10^{-3}
0.9	-8841.1137	5.5170×10^{-5}	2.6742×10^{-3}	2.9395×10^{-3}
1.0 (P)	-8844.2078	9.1753×10^{-7}	2.5801×10^{-3}	3.0105×10^{-3}

Table 5: Energy, gradient norm and first two eigenvalues of $(MgO)_{12}$ cluster at each P_c

P_c	**Energy (in kJ/mol)**	**Gradient norm**	**First eigenvalue**	**Second eigenvalue**
0.0 (R)	-10317.1226	1.8850×10^{-9}	8.7342×10^{-4}	1.3281×10^{-3}
0.1043	-10316.7704	2.4056×10^{-6}	8.8193×10^{-4}	1.3439×10^{-3}
0.2086	-10315.6712	1.0302×10^{-5}	7.8061×10^{-4}	1.3308×10^{-3}
0.3127	-10313.8867	2.0797×10^{-5}	5.5614×10^{-4}	1.2876×10^{-3}
0.4170	-10311.6423	2.8199×10^{-5}	1.5774×10^{-4}	1.2093×10^{-3}
0.5215	-10309.4264	2.8818×10^{-5}	-4.3953×10^{-4}	1.0892×10^{-3}
0.6266	-10307.8823	2.2566×10^{-5}	-1.1062×10^{-3}	9.1608×10^{-4}
0.7317	-10307.1259	1.8918×10^{-6}	-1.5260×10^{-3}	7.7956×10^{-4}
0.7847 (TS)	-10307.1188	2.0472×10^{-8}	-1.4970×10^{-3}	7.8735×10^{-4}
0.8382	-10307.4083	1.6159×10^{-6}	-1.0209×10^{-3}	9.2157×10^{-4}
0.9461	-10308.5166	1.5010×10^{-6}	1.1657×10^{-3}	1.6175×10^{-3}
1.0 (P)	-10308.7138	2.5984×10^{-7}	1.1965×10^{-3}	1.9204×10^{-3}

Table 6: Energy, gradient norm and first two eigenvalues of $(MgO)_{14}$ cluster at each P_c

P_c	**Energy (in kJ/mol)**	**Gradient norm**	**First eigenvalue**	**Second eigenvalue**
0.0 (R)	-15654.1949	3.7872×10^{-8}	6.0922×10^{-4}	1.2554×10^{-3}
0.1	-15653.7107	2.4779×10^{-6}	5.1056×10^{-4}	1.2185×10^{-3}
0.2	-15652.5152	8.5372×10^{-6}	3.8623×10^{-4}	1.1701×10^{-3}
0.3	-15650.7523	2.4936×10^{-5}	1.9622×10^{-4}	1.0884×10^{-3}
0.4	-15649.0147	3.2064×10^{-5}	-1.0226×10^{-4}	9.3387×10^{-4}
0.5	-15647.8865	1.7381×10^{-5}	-5.4406×10^{-4}	6.6105×10^{-4}
0.55	-15647.7323	3.4248×10^{-6}	-8.1620×10^{-4}	4.8561×10^{-4}
0.6002(TS)	-15647.6623	5.4342×10^{-10}	-1.0957×10^{-3}	3.0012×10^{-4}
0.65	-15647.7979	3.3368×10^{-7}	-1.2620×10^{-3}	1.7969×10^{-4}
0.7	-15648.2771	1.4248×10^{-6}	-1.3194×10^{-3}	1.2987×10^{-4}
0.8	-15650.3362	6.6709×10^{-6}	-6.9023×10^{-4}	6.0244×10^{-4}
0.9	-15652.8319	3.3826×10^{-5}	1.2802×10^{-3}	1.6611×10^{-3}
1.0 (P)	-15654.3813	1.4482×10^{-8}	1.2878×10^{-3}	1.7772×10^{-3}

Table 7: Energy, gradient norm and first two eigenvalues of $(MgO)_{21}$ cluster at each P_c

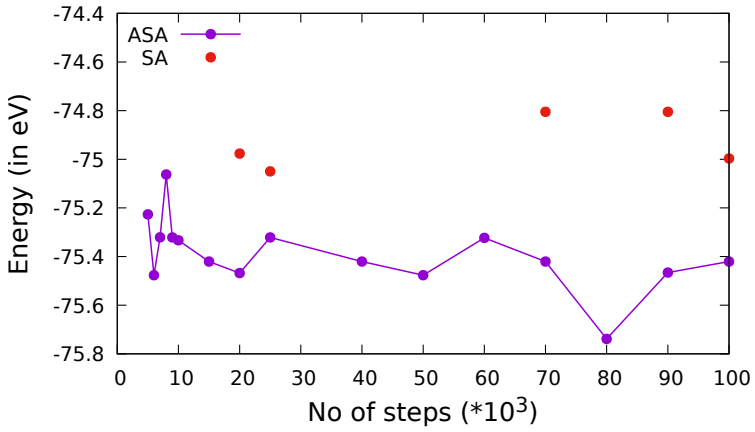

Figure 1: Comparison of SA and ASA for $(MgO)_{10}$ cluster. For a few step counts, no valid SA structure corresponding to an ASA structure was found. Furthermore, ASA yielded the global minimum at step count = 80000. This clearly shows that ASA is the superior algorithm.

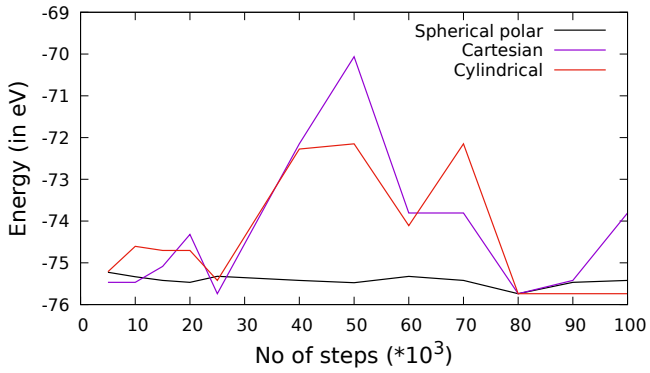

(a) $(MgO)_{10}$

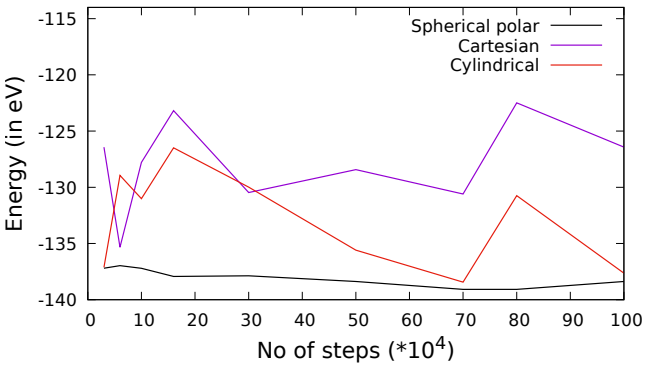

(b) $(MgO)_{18}$

Figure 2: Comparison of the performance of the ASA algorithm using three different coordinate systems. While the cartesian and cylindrical coordinate systems follow an uneven, irregular trend, the spherical coordinate system consistently yields low energy structures. Clearly, the spherical coordinate system is the best choice to not only locate the global minimum for a particular cluster, but also stable local minima. For this comparison, ASA was used throughout.

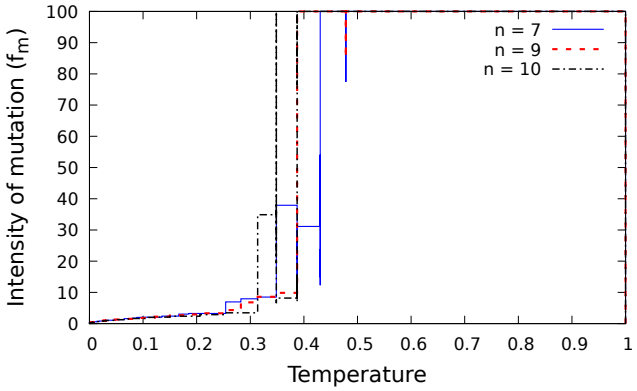

(a)

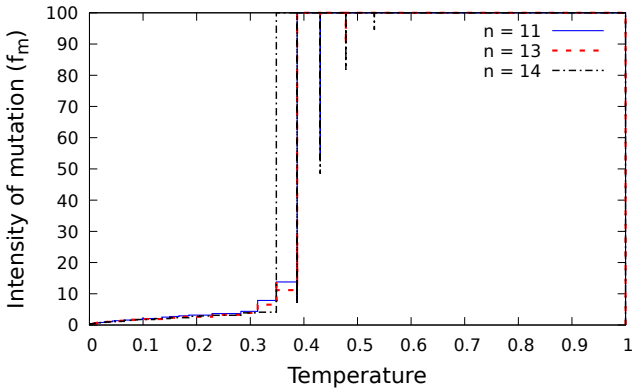

(b)

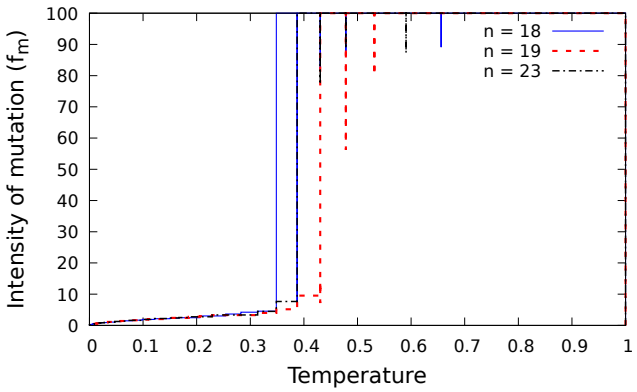

(c)

Figure 3: Variation of intensity of mutation f_m with temperature for a few extra sizes

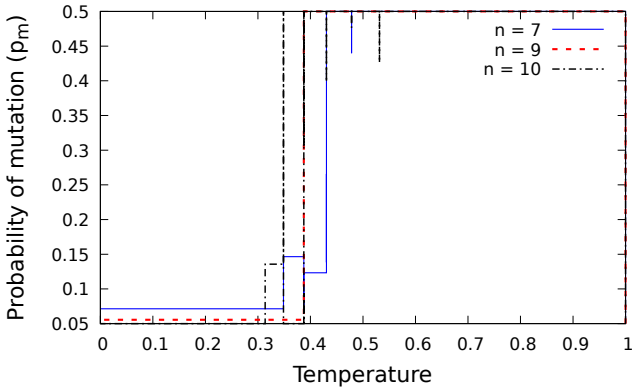

(a)

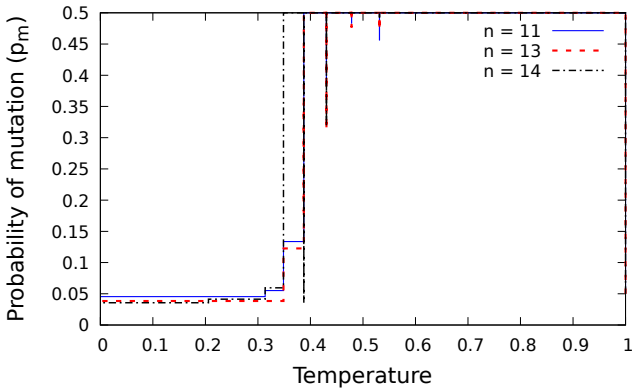

(b)

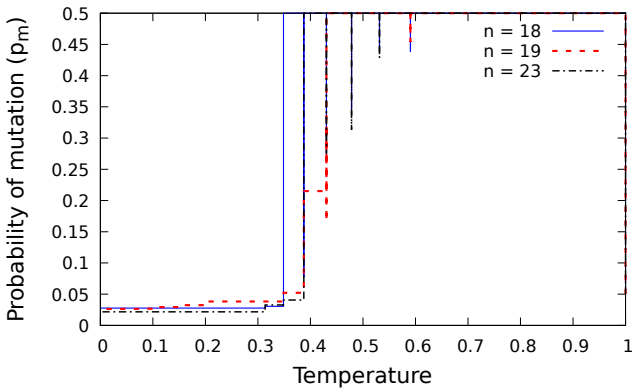

(c)

Figure 4: Variation of probability of mutation p_m with temperature for a few extra sizes

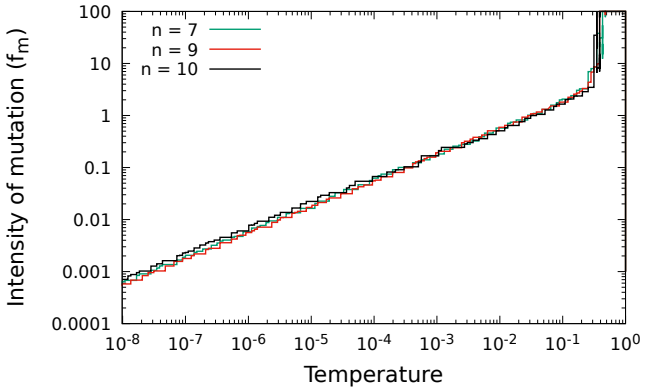

(a)

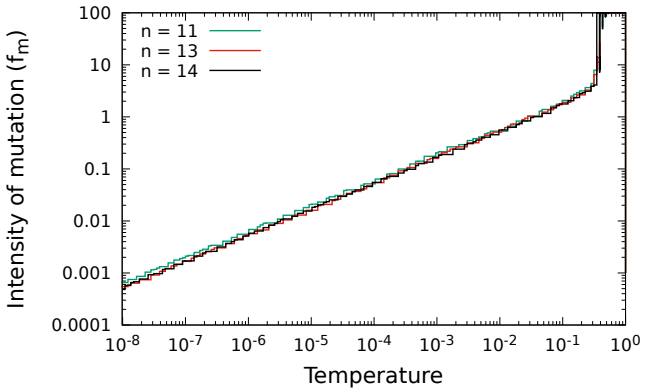

(b)

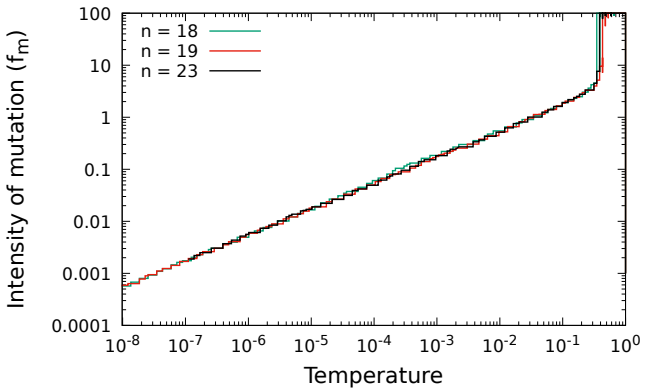

(c)

Figure 5: Variation of f_m in the logarithmic scale so as to clearly depict the changes at low ranges

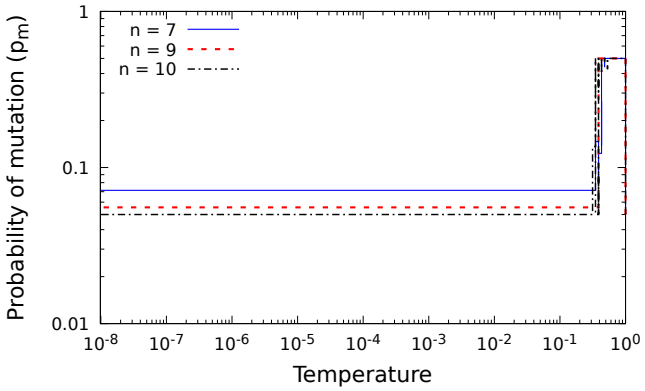

(a)

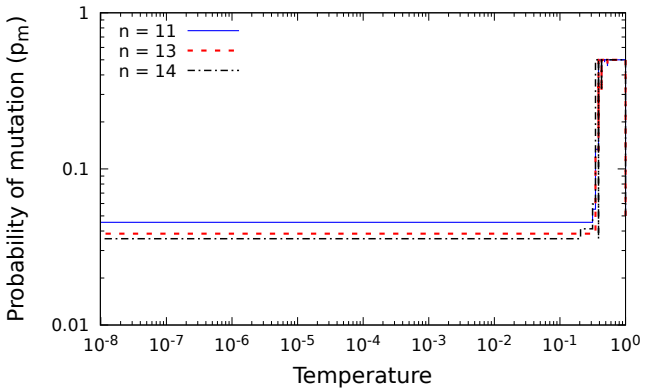

(b)

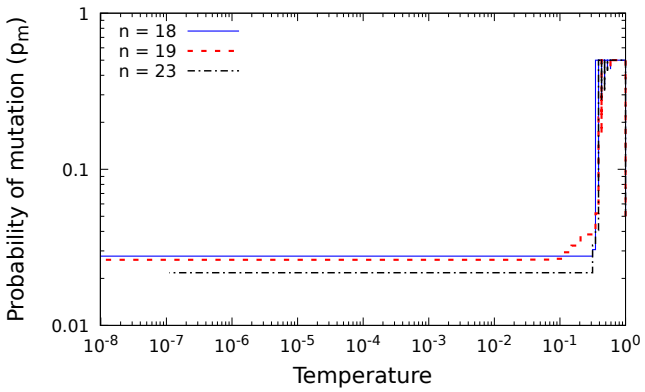

(c)

Figure 6: Variation of p_m in the logarithmic scale so as to clearly depict the changes at low ranges

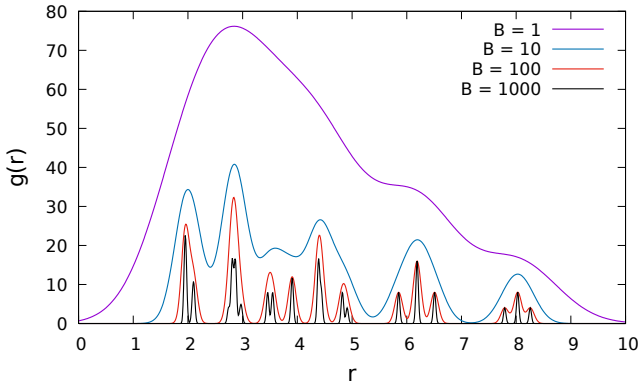

(a) $(MgO)_{10}$

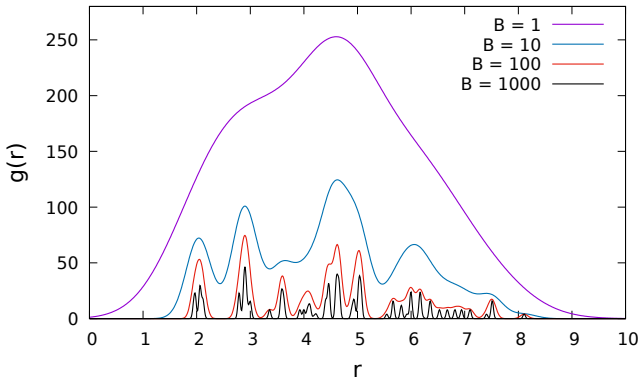

(b) $(MgO)_{18}$

Figure 7: Variation in the Radial Distribution Function (RDF) with the value of the soothening parameter, B for two sizes

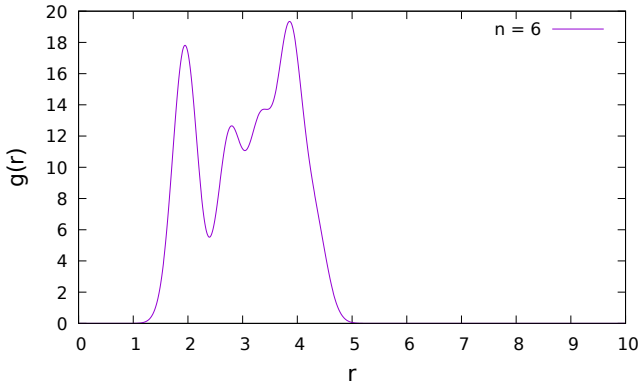

(a) $(MgO)_6$

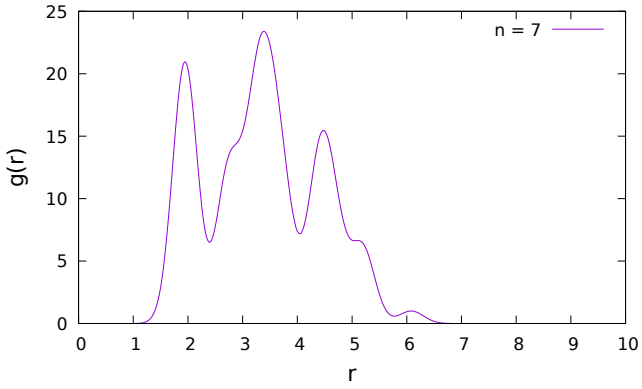

(b) $(MgO)_7$

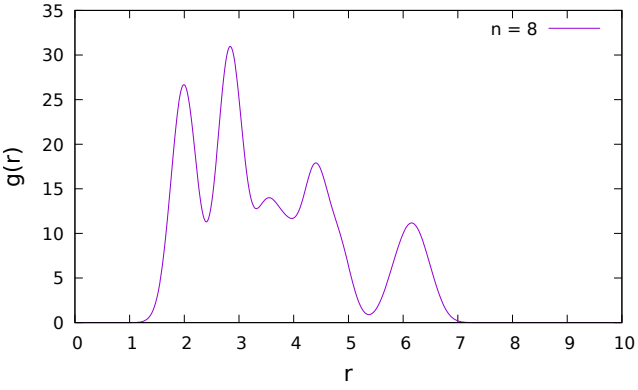

(c) $(MgO)_8$

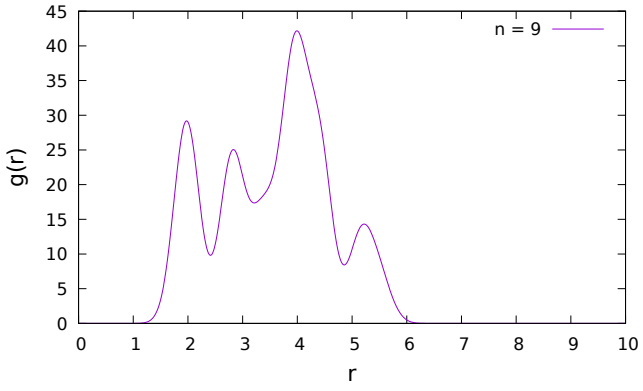

(d) $(MgO)_9$

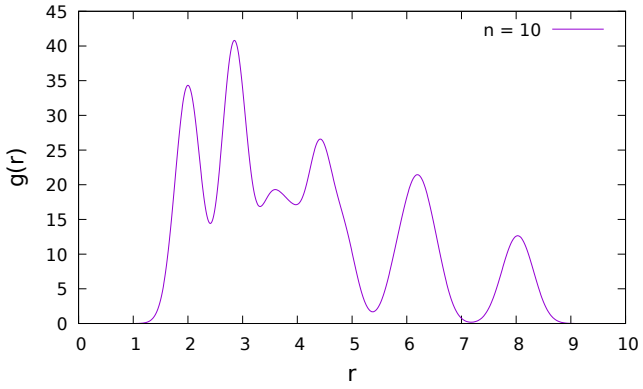

(e) $(MgO)_{10}$

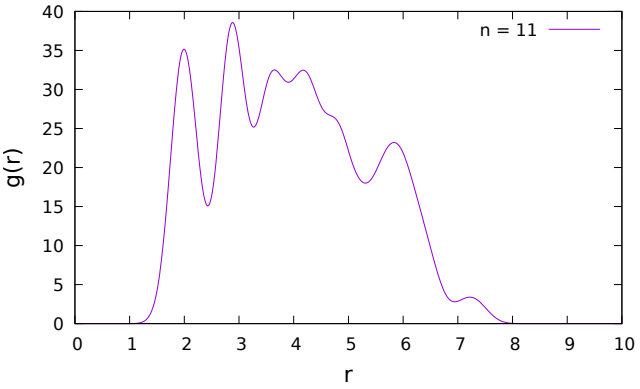

(f) $(MgO)_{11}$

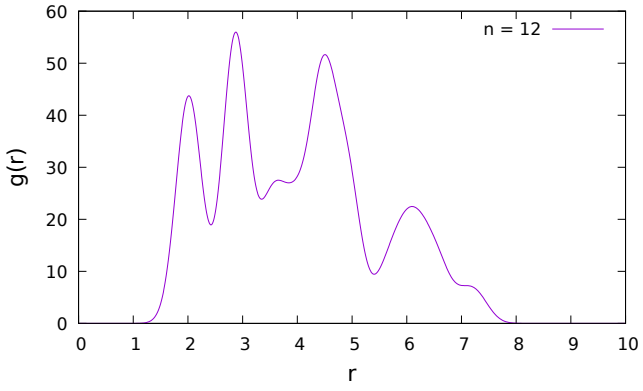

(g) $(MgO)_{12}$

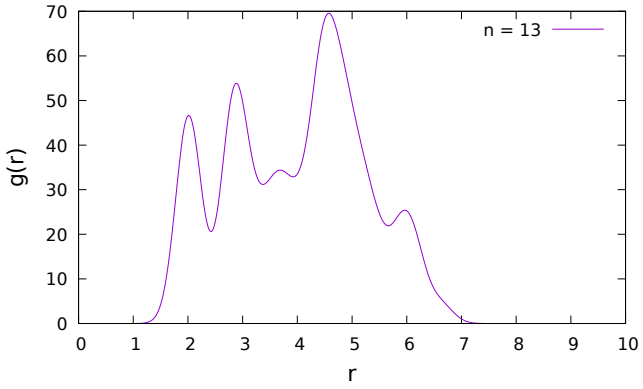

(h) $(MgO)_{13}$

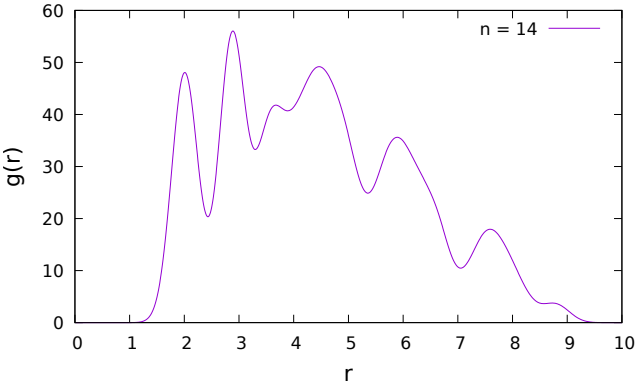

(i) $(MgO)_{14}$

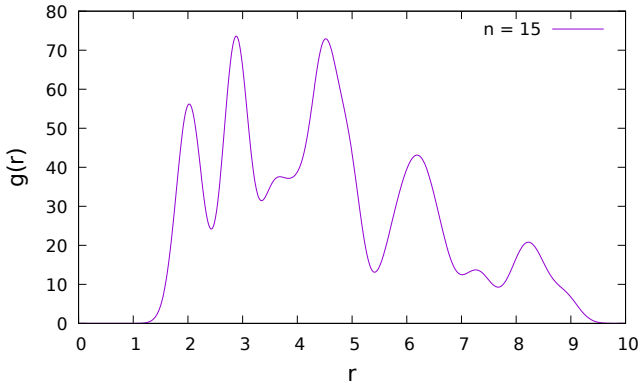

(j) $(MgO)_{15}$

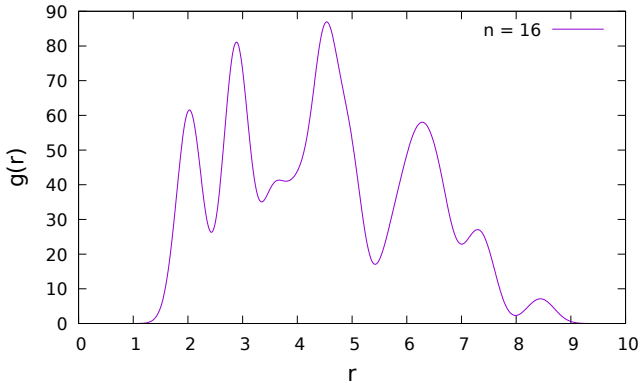

(k) $(MgO)_{16}$

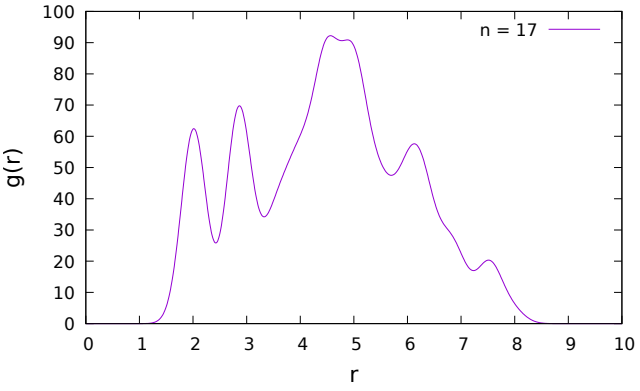

(l) $(MgO)_{17}$

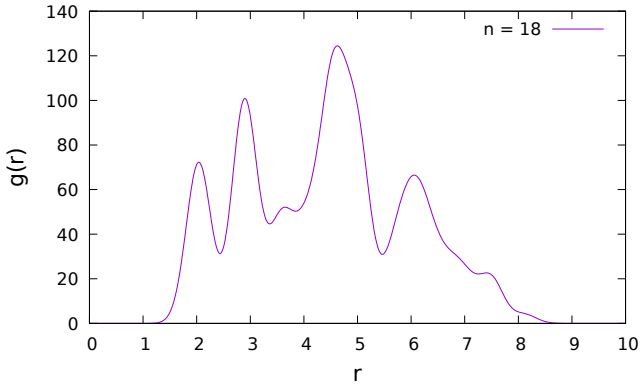

(m) $(MgO)_{18}$

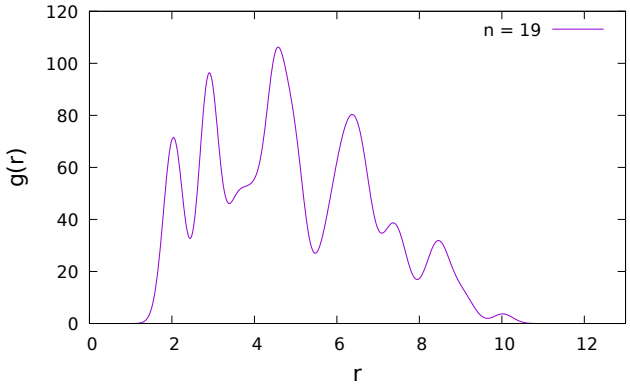

(n) $(MgO)_{19}$

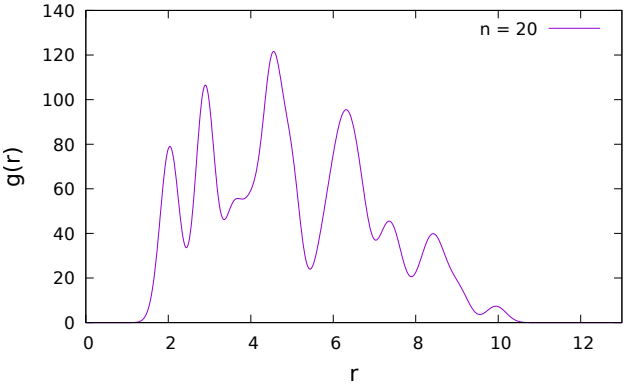

(o) $(MgO)_{20}$

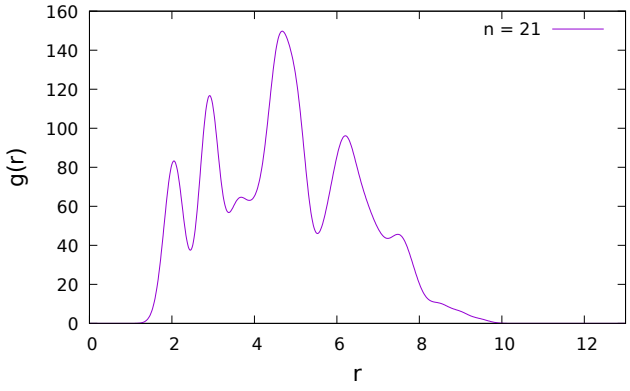

(p) $(MgO)_{21}$

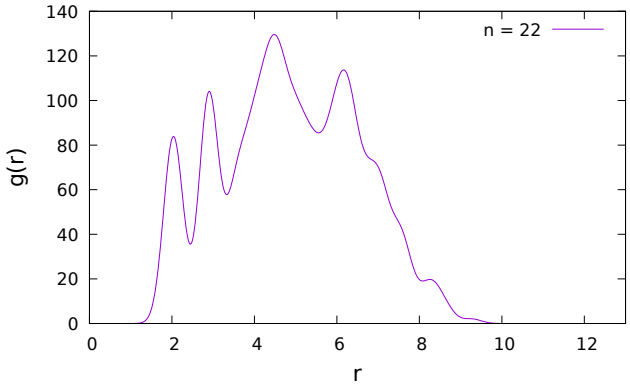

(q) $(MgO)_{22}$

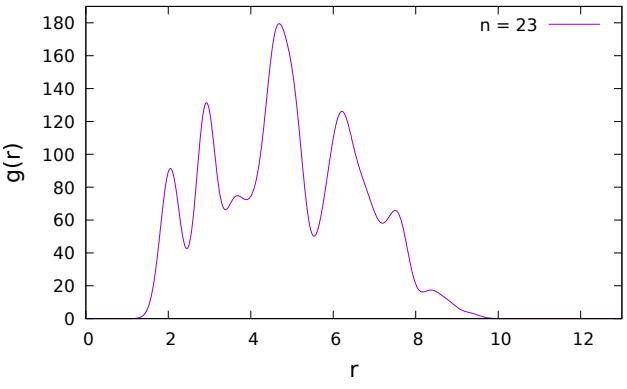

(r) $(MgO)_{23}$

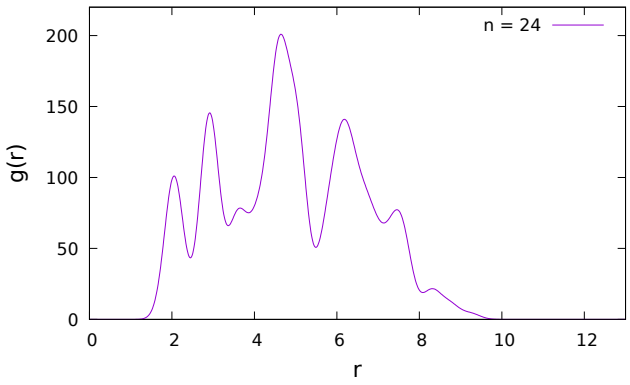

(s) $(MgO)_{24}$

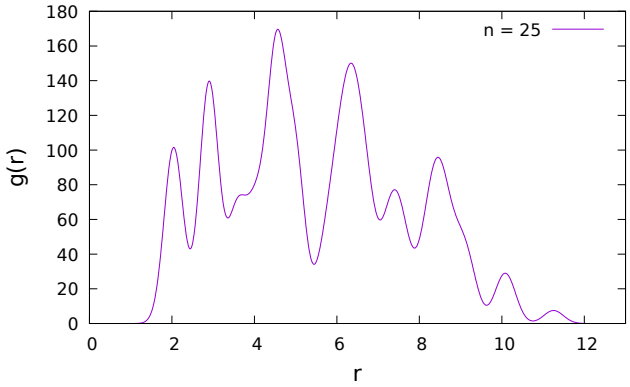

(t) $(MgO)_{25}$

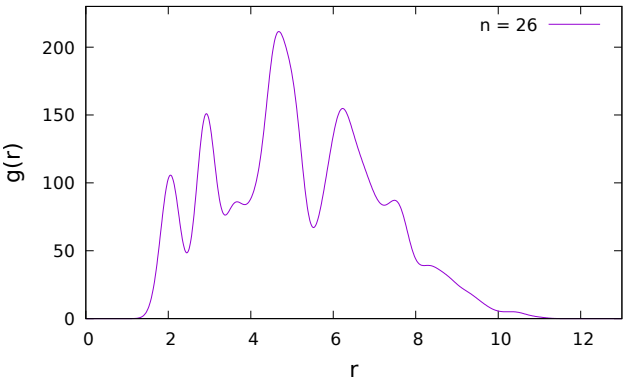

(u) $(MgO)_{26}$

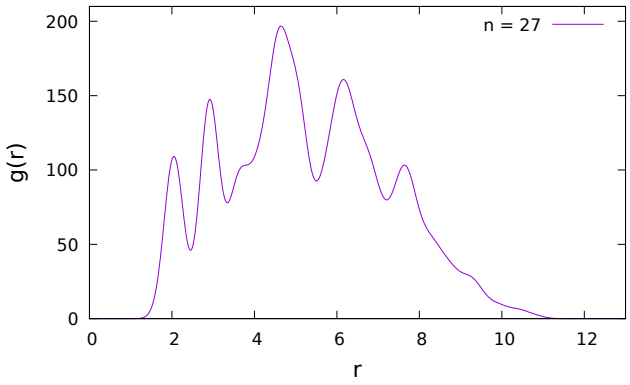

(v) $(MgO)_{27}$

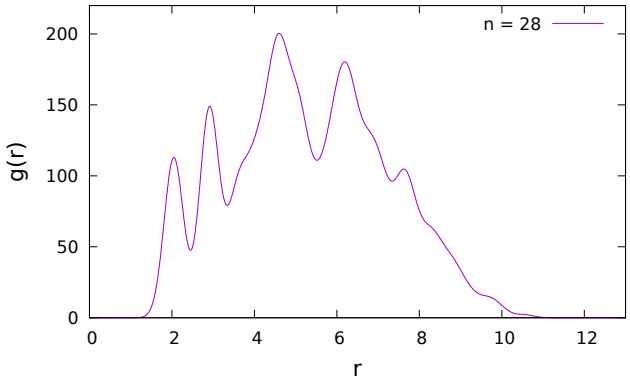

(w) $(MgO)_{28}$

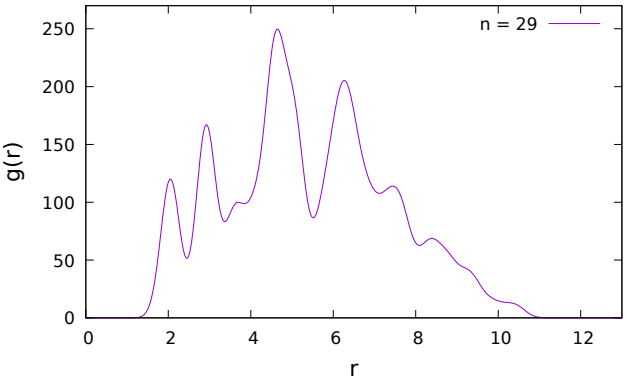

(x) $(MgO)_{29}$

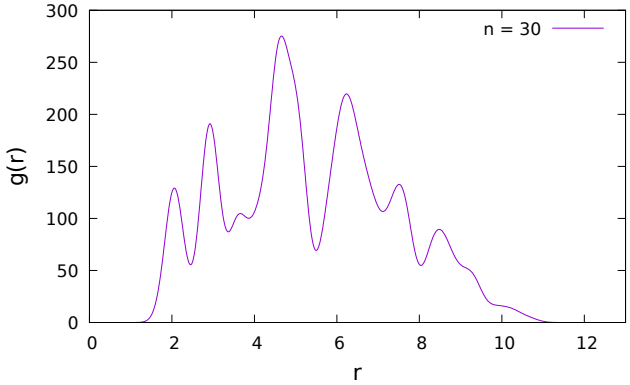

(y) $(MgO)_{30}$

Figure 8: Radial Distribution Functions (RDF) for all the global structures as generated by the ASA algorithm using the Born-Mayer potential

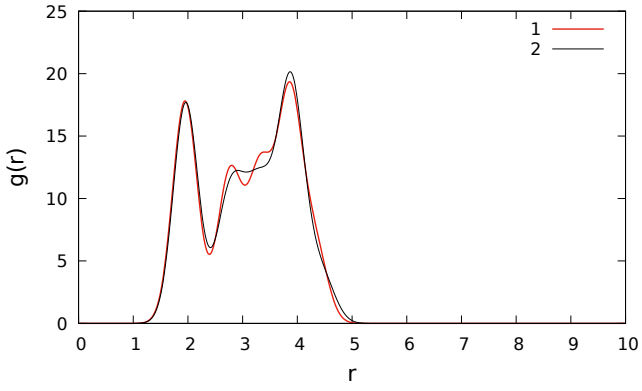

(a) $(MgO)_6$

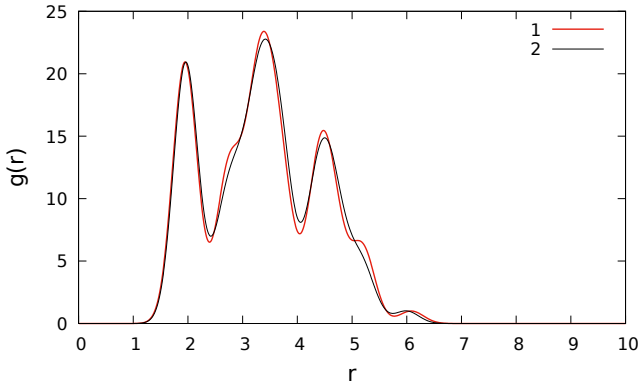

(b) $(MgO)_7$

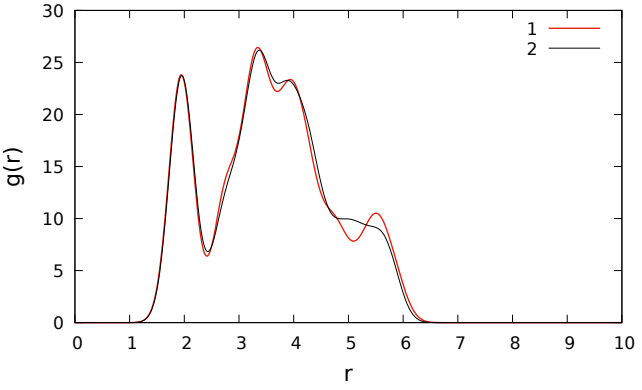

(c) $(MgO)_8$ (Local)

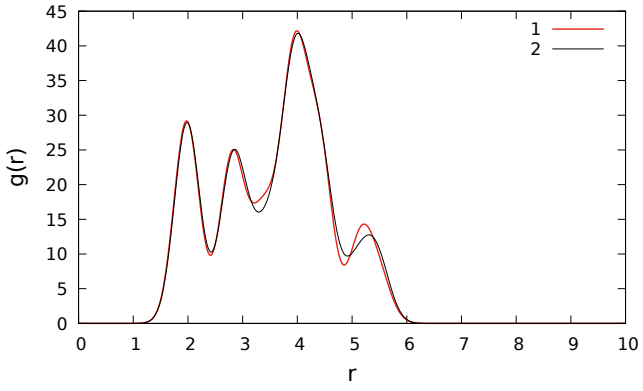

(d) $(MgO)_9$

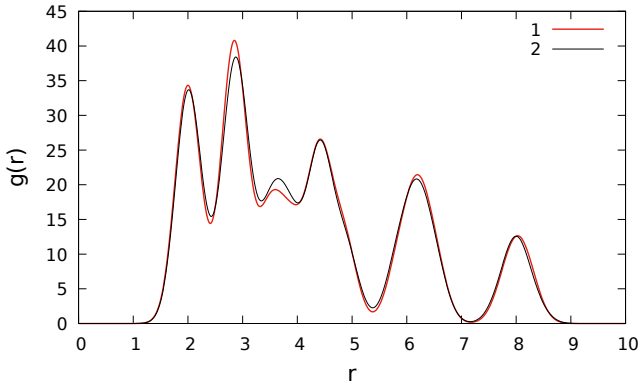

(e) $(MgO)_{10}$

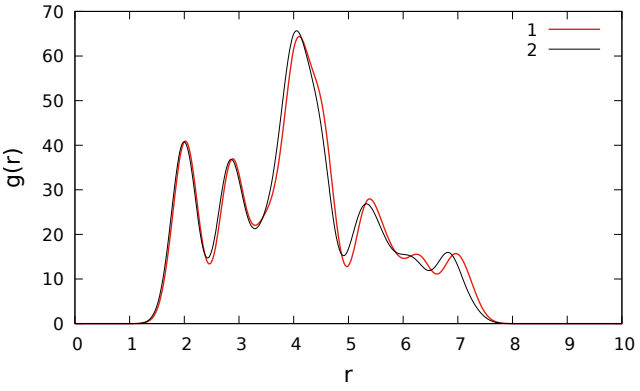

(f) $(MgO)_{12}$ (Local)

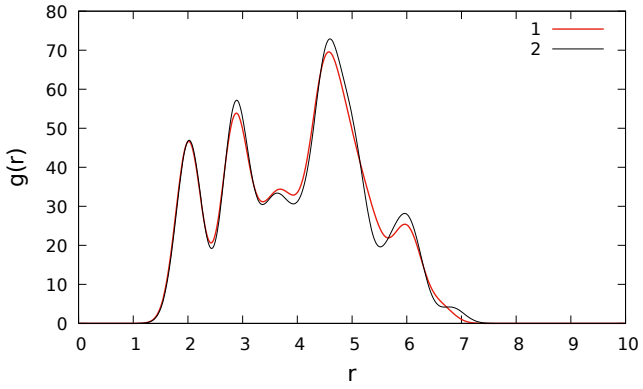

(g) $(MgO)_{13}$

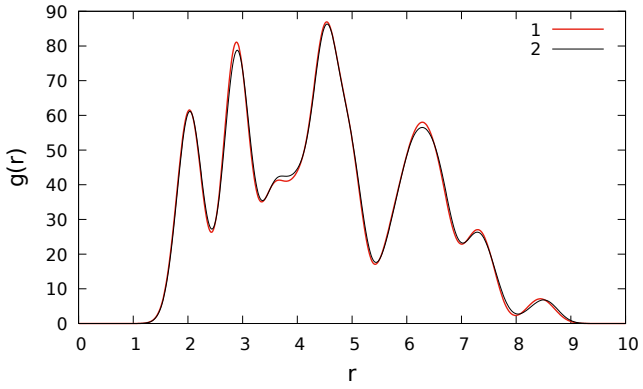

(h) $(MgO)_{16}$

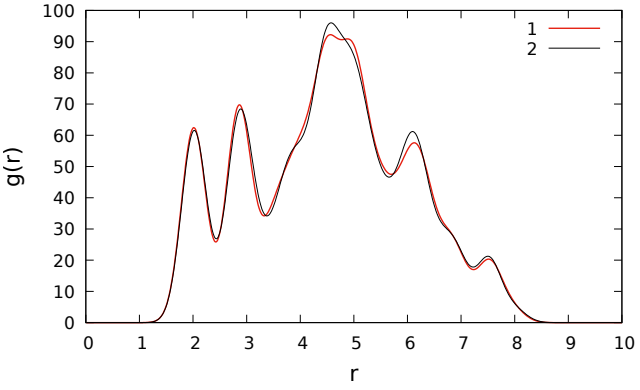

(i) $(MgO)_{17}$

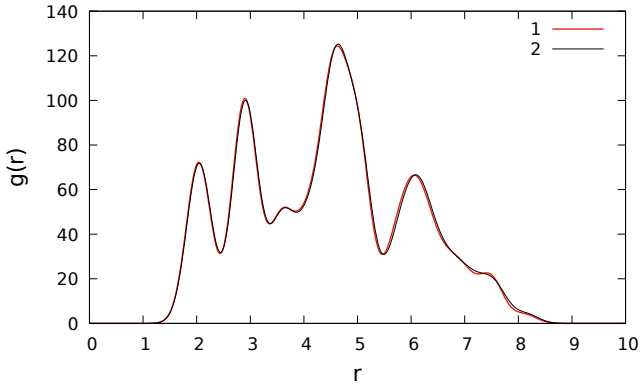

(j) $(MgO)_{18}$

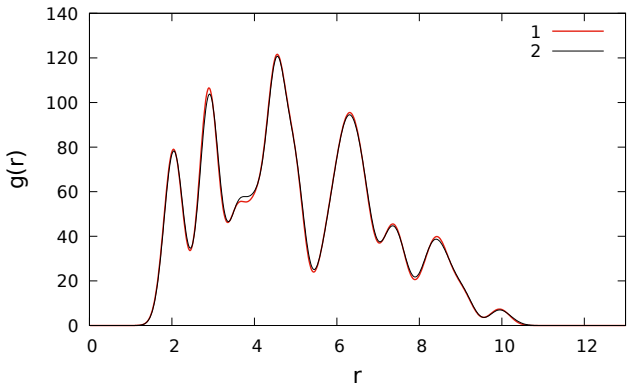

(k) $(MgO)_{20}$

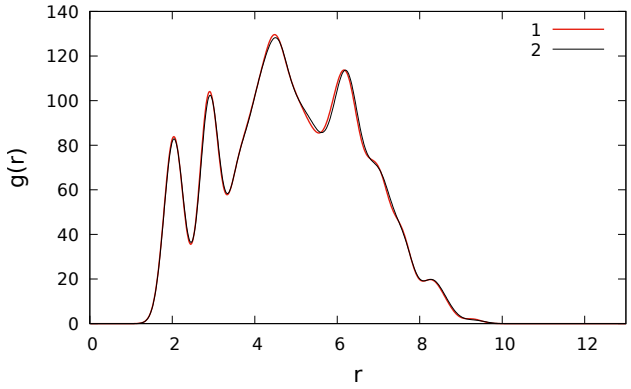

(l) $(MgO)_{22}$

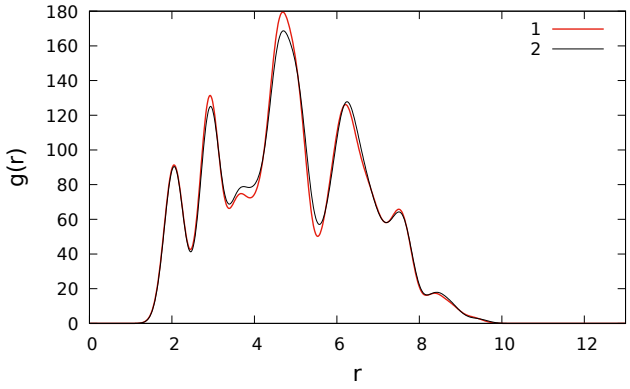

(m) $(MgO)_{23}$

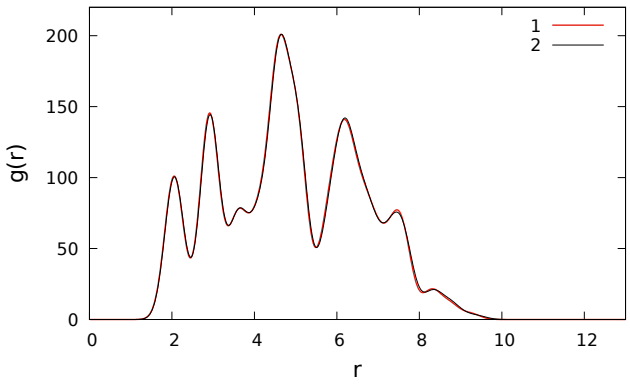

(n) $(MgO)_{24}$

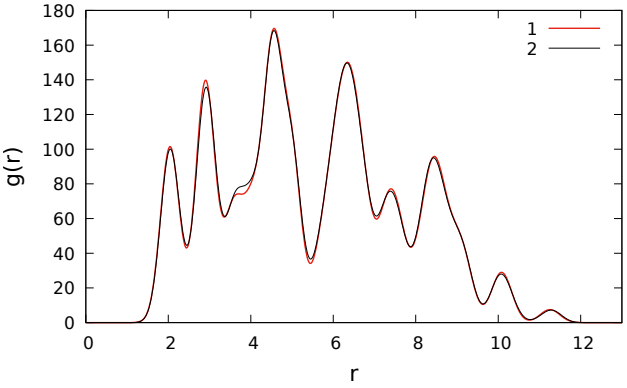

(o) $(MgO)_{25}$

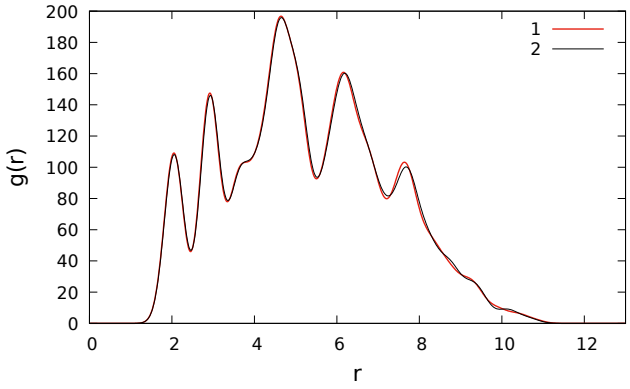

(p) $(MgO)_{27}$

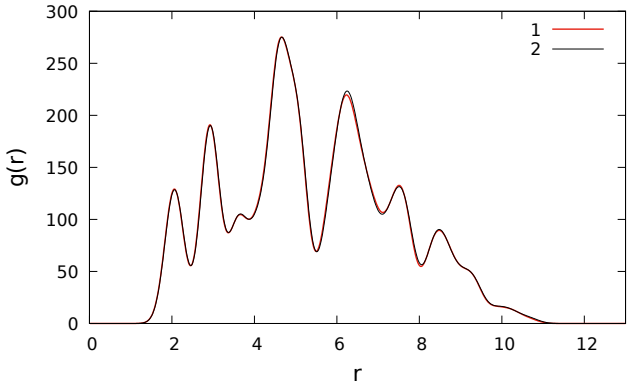

(q) $(MgO)_{30}$

Figure 9: Comparison of the Radial Distribution Functions (RDF) of our ASA generated structures (1) to the DFT optimised coordinates (2) reported by Dixon et al. (optimised at the B3LYP/DZVP level). The similarity between the two clearly proves that our stochastic optimisation process has a high level of accuracy and that the Born-Mayer potential can describe $(MgO)_n$ clusters to a very good extent.

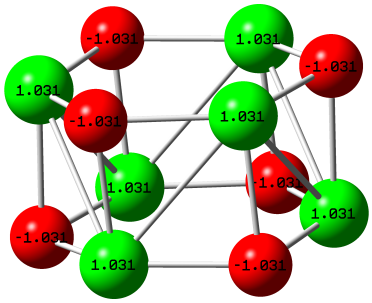

(a) $(MgO)_6$

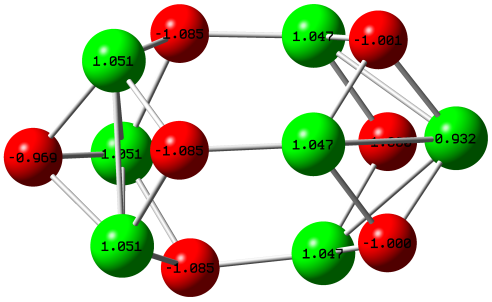

(b) $(MgO)_7$

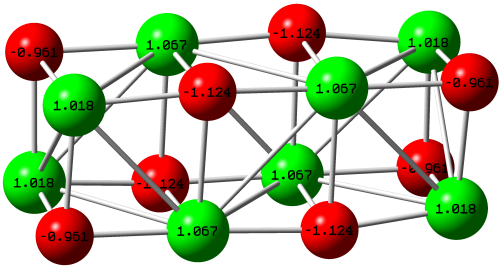

(c) $(MgO)_8$

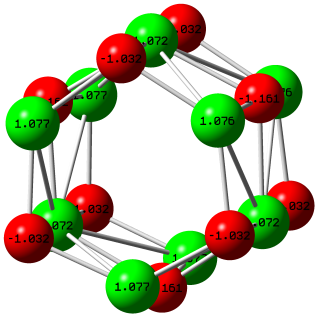

(d) $(MgO)_9$

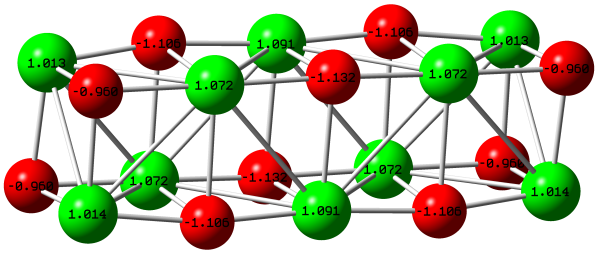

(e) $(MgO)_{10}$

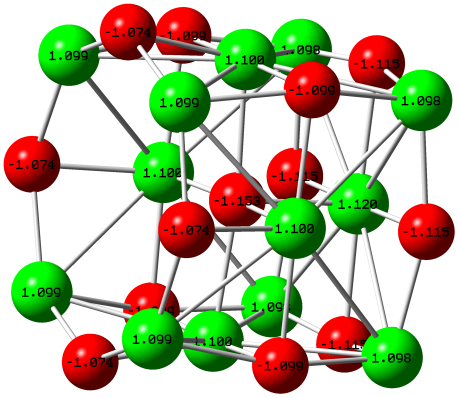

(f) $(MgO)_{13}$

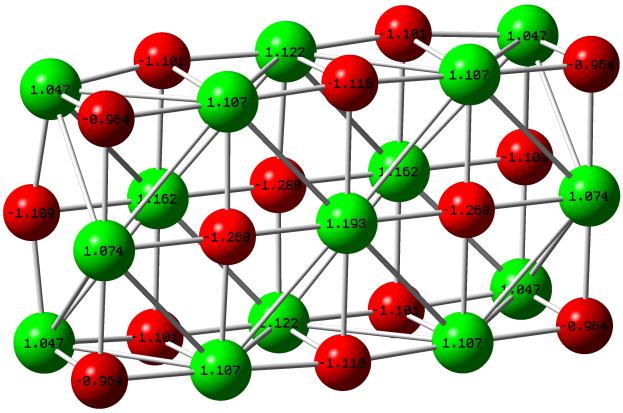

(g) $(MgO)_{15}$

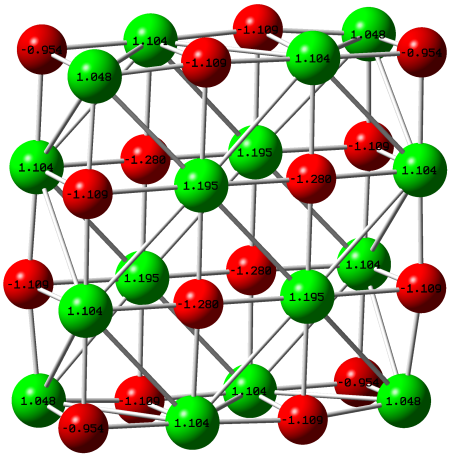

(h) $(MgO)_{16}$

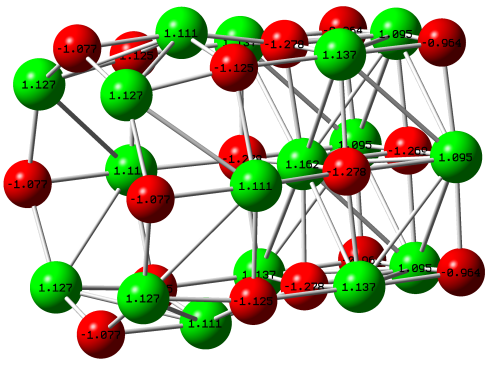

(i) $(MgO)_{17}$

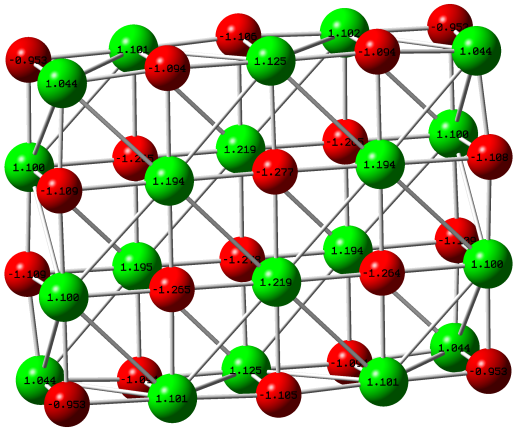

(j) $(MgO)_{20}$

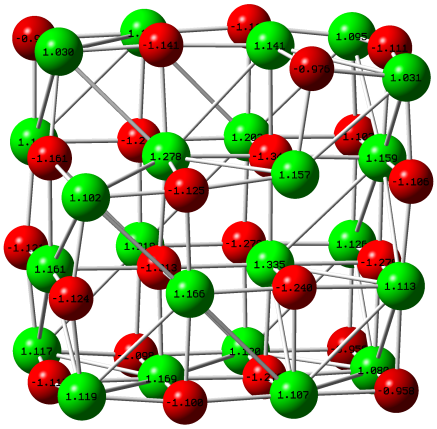

(k) $(MgO)_{23}$

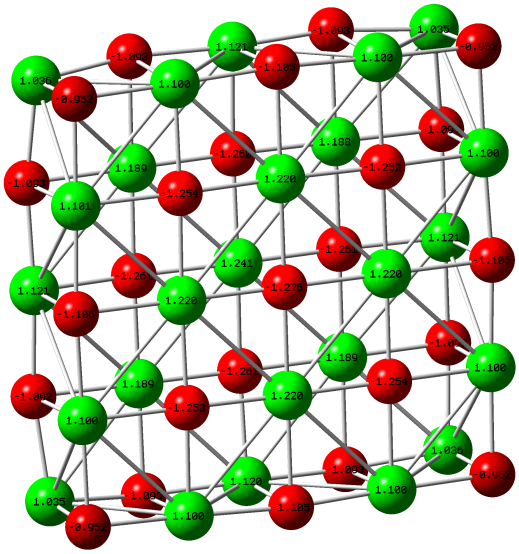

(l) $(MgO)_{25}$

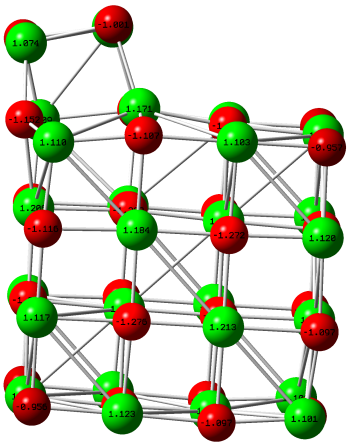

(m) $(MgO)_{26}$

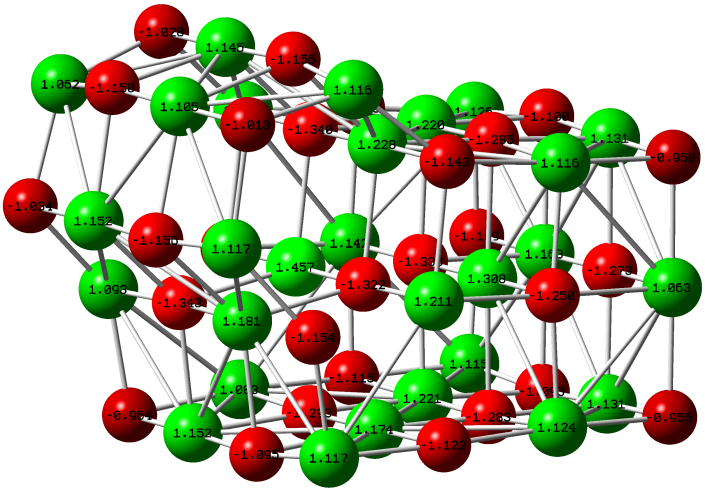

(n) $(MgO)_{28}$

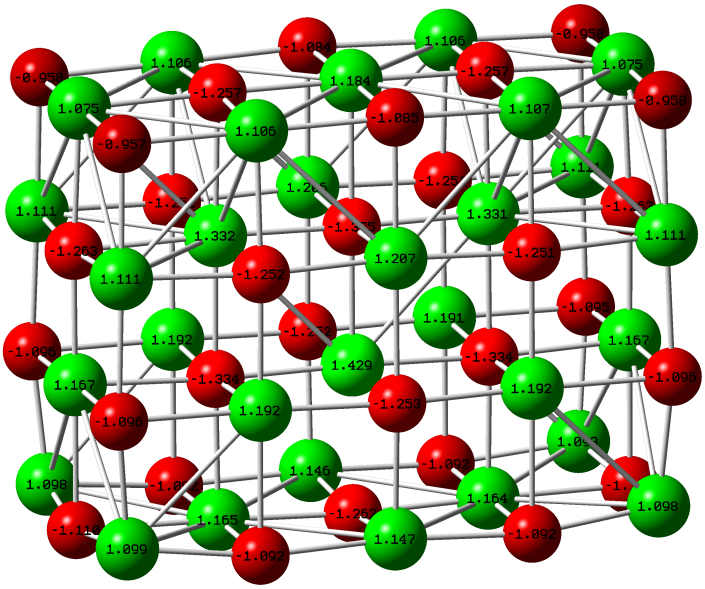

(o) $(MgO)_{30}$

Figure 10: DFT optimised lowest energy isomers of $(MgO)_n$ clusters, with exact ionic charges on the atoms

Cluster Size (n)	**Haertelt**	**Dixon**	**ASA + DFT** (present work)
6	-1652.463624	**-1652.463730**	-1652.463671
7	**-1927.876613**	-1927.876600	-1927.876592
8	-2203.357437	**-2203.357456**	-2203.352968
9	-2478.842728	**-2478.842794**	-2478.842684
10	-2754.249106	**-2754.253891**	-2754.253890
11	**-3029.719998**	-3029.719993	-3029.711463
12	-3305.212706	**-3305.220303**	-3305.200402
13	-3580.611263	**-3580.622617**	-3580.619697
14	-3856.079327	**-3856.087799**	-3856.085647
15	-4131.597204	**-4131.597453**	-4131.577035
16	-4407.046163	-4407.051660	**-4407.051704**
17	NA	**-4682.482874**	-4682.475921
18	NA	**-4957.986593**	-4957.986534
19	NA	**-5233.400400**	-5233.391358
20	NA	-5508.904240	**-5508.904243**
21	NA	**-5784.351313**	-5784.328743
22	NA	**-6059.824604**	-6059.824603
23	NA	**-6335.273781**	-6335.264719
24	NA	-6610.817547	**-6610.817556**
25	NA	**-6886.232592**	-6886.232485
26	NA	-7161.660806	**-7161.665915**
27	NA	**-7437.177696**	-7437.177407
28	NA	-7712.638850	**-7712.650118**
29	NA	-7988.052041	**-7988.078431**
30	NA	-8263.632594	**-8263.632598**

Table 8: Energies (in Hartree) of the global minima of $(MgO)_n$ clusters as obtained in different works (re-optimised at the B3LYP/DGTZVP level of theory)

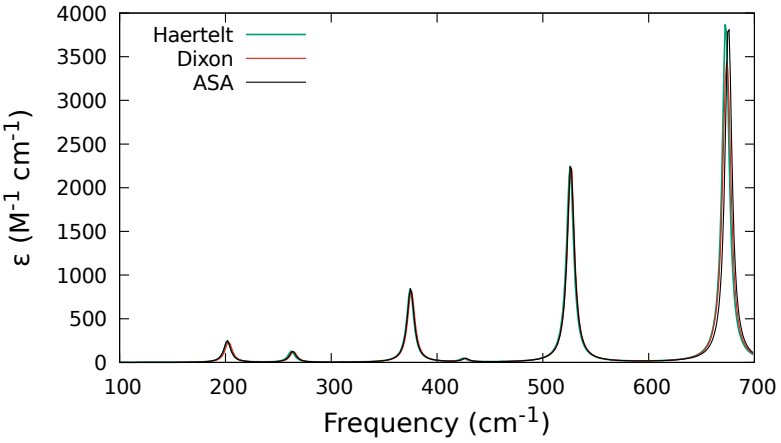

(a) $(MgO)_6$

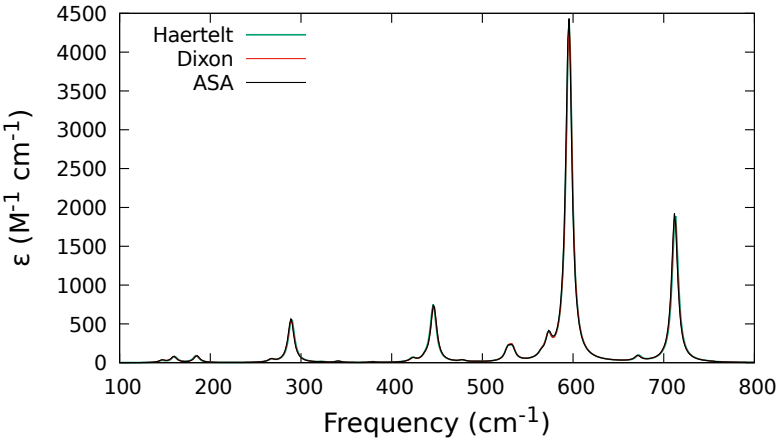

(b) $(MgO)_7$

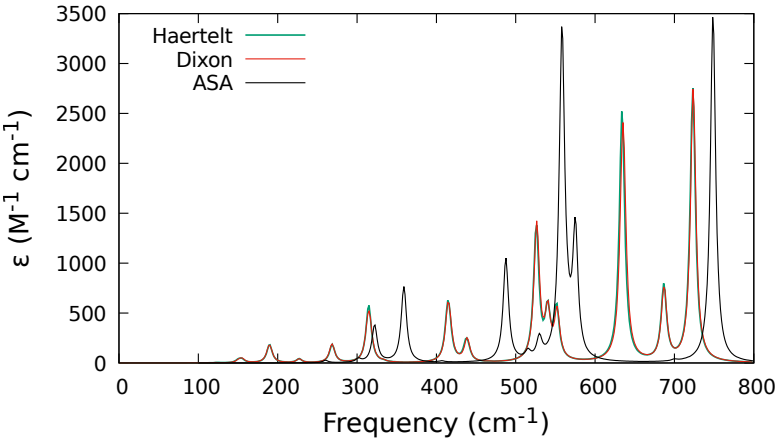

(c) $(MgO)_8$

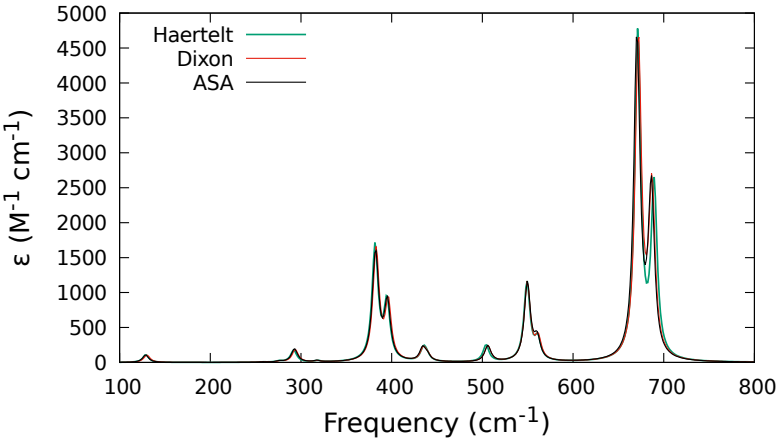

(d) $(MgO)_9$

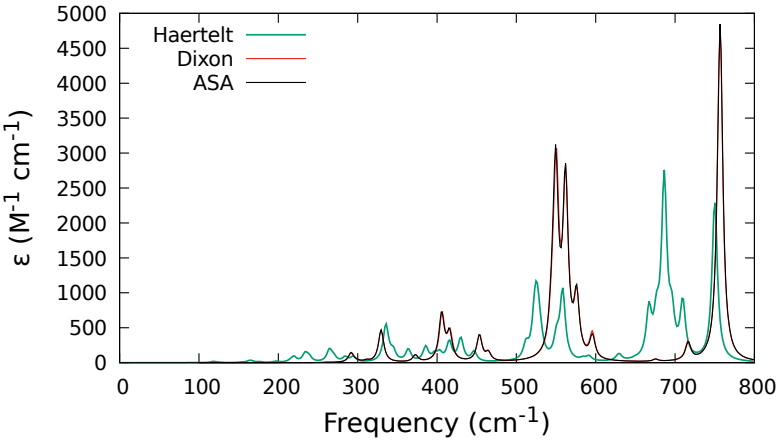

(e) $(MgO)_{10}$

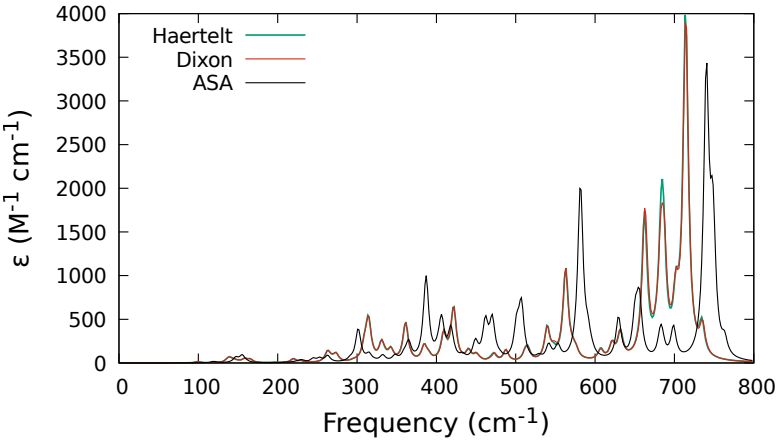

(f) $(MgO)_{11}$

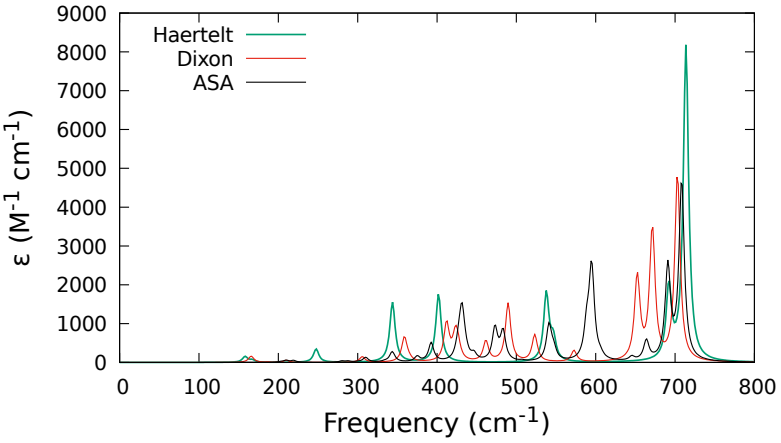

(g) $(MgO)_{12}$

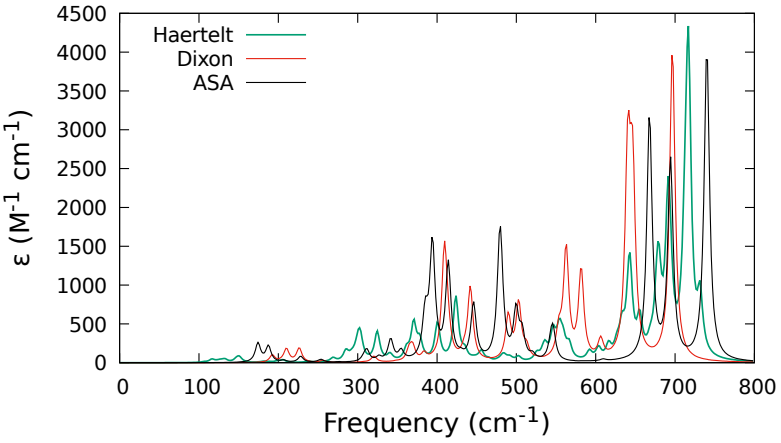

(h) $(MgO)_{13}$

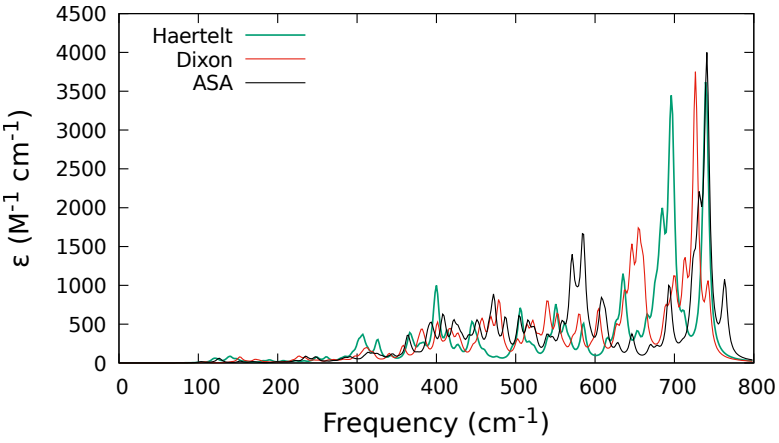

(i) $(MgO)_{14}$

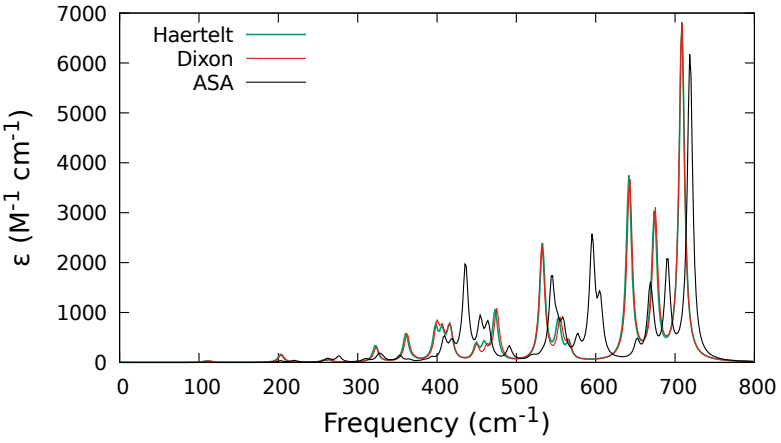

(j) $(MgO)_{15}$

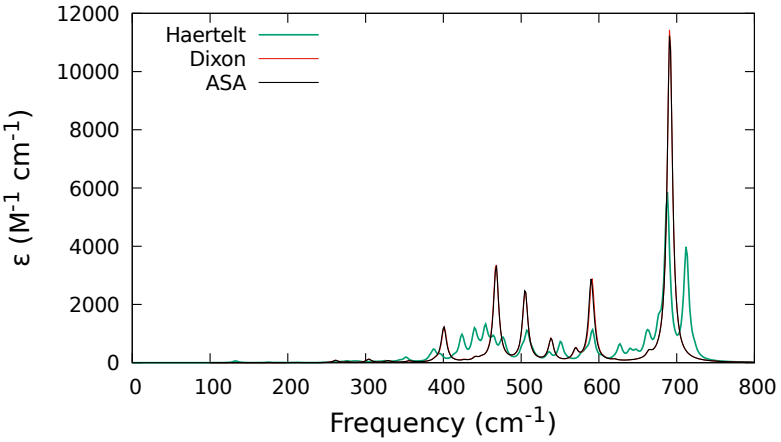

(k) $(MgO)_{16}$

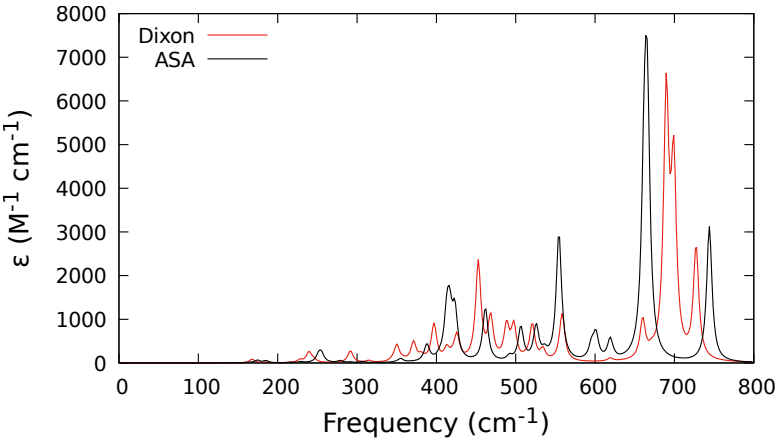

(l) $(MgO)_{17}$

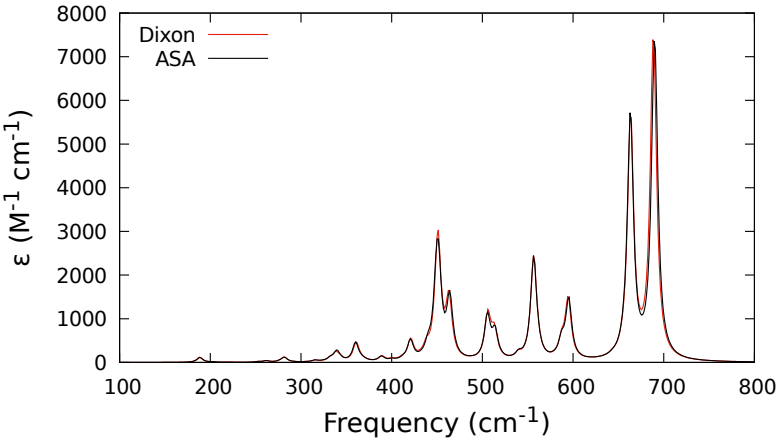

(m) $(MgO)_{18}$

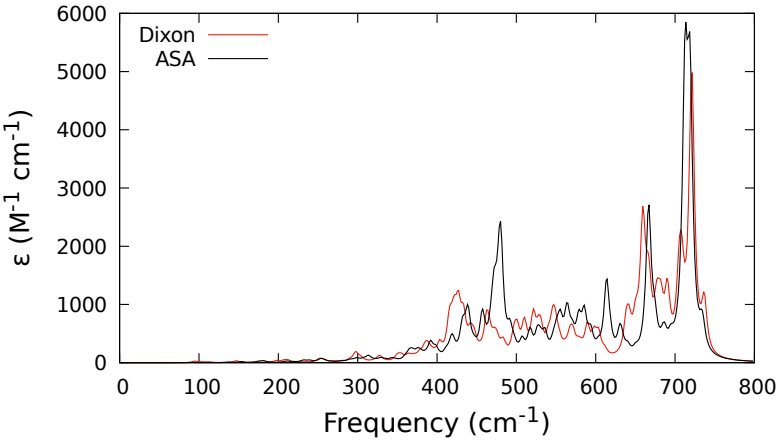

(n) $(MgO)_{19}$

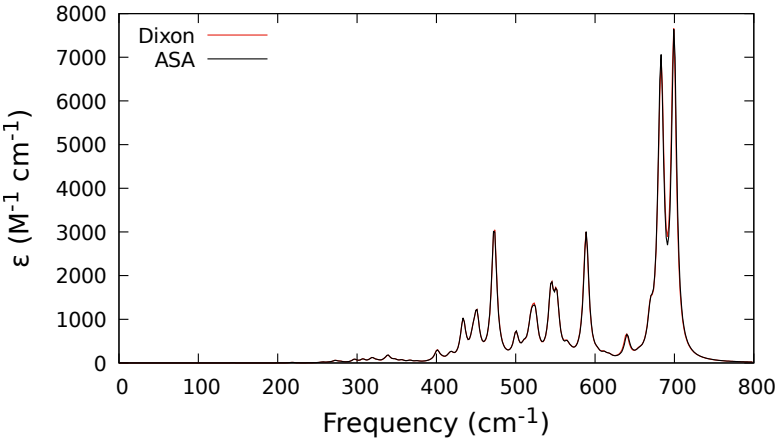

(o) $(MgO)_{20}$

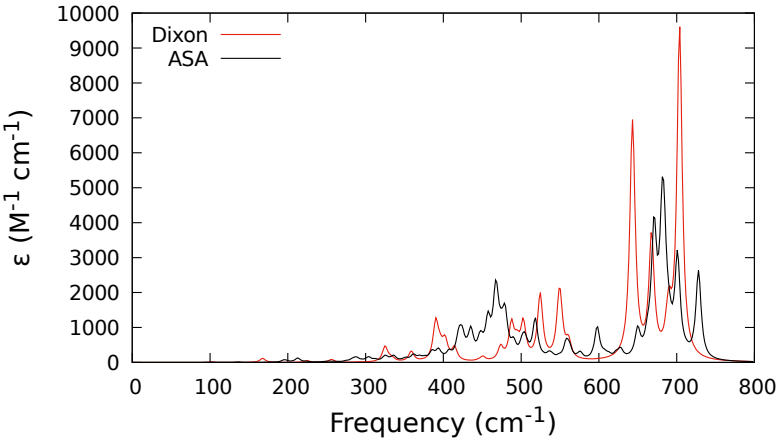

(p) $(MgO)_{21}$

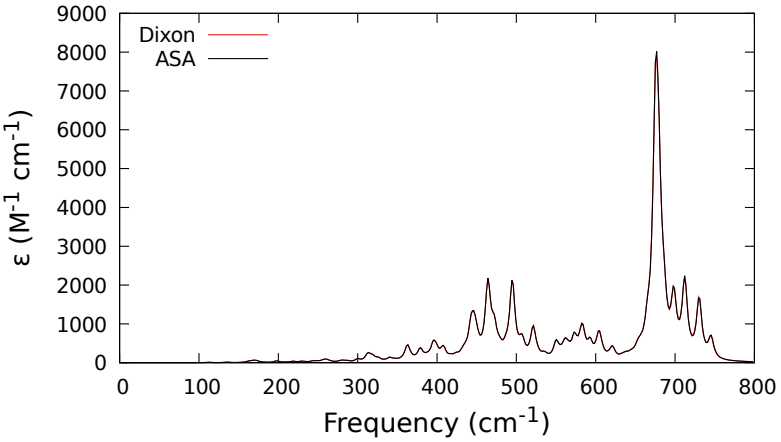

(q) $(MgO)_{22}$

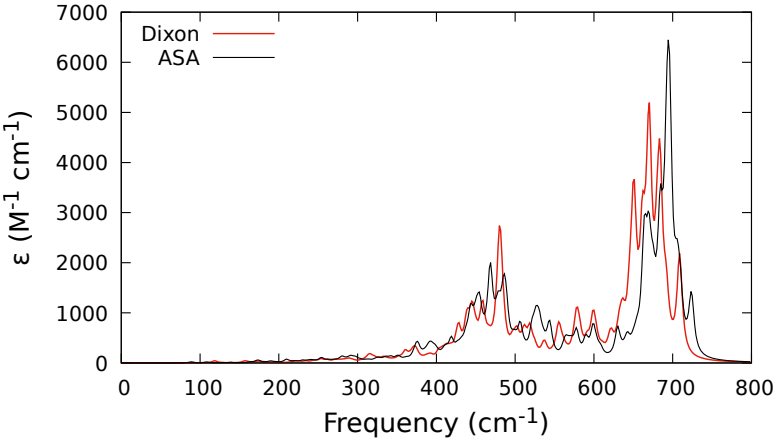

(r) $(MgO)_{23}$

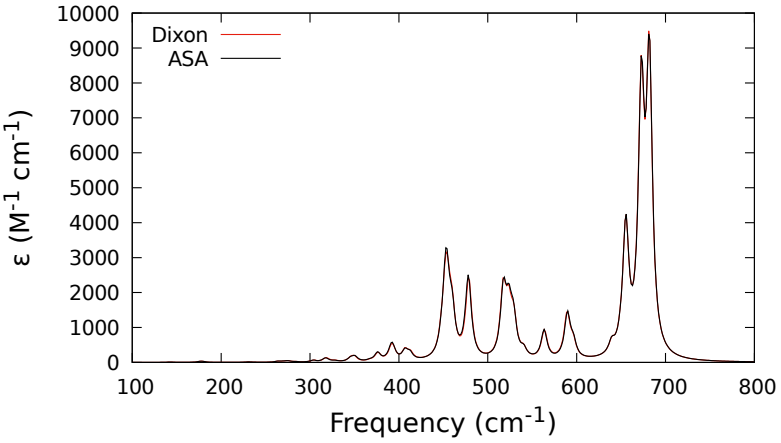

(s) $(MgO)_{24}$

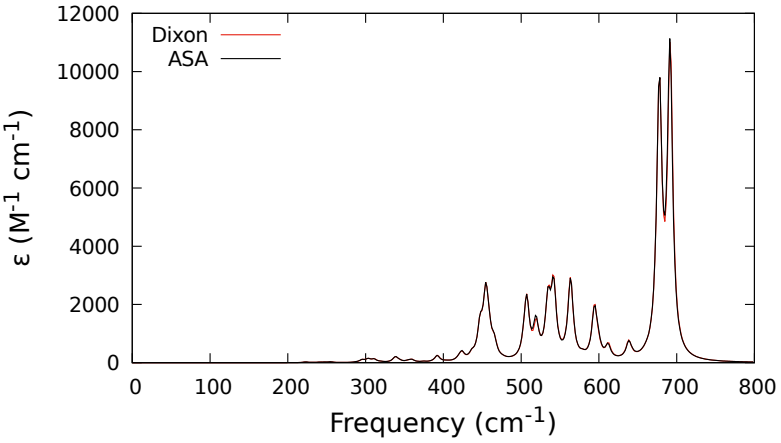

(t) $(MgO)_{25}$

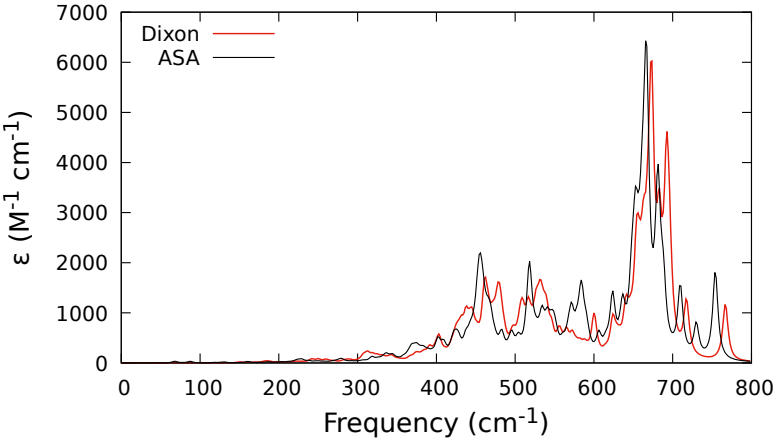

(u) $(MgO)_{26}$

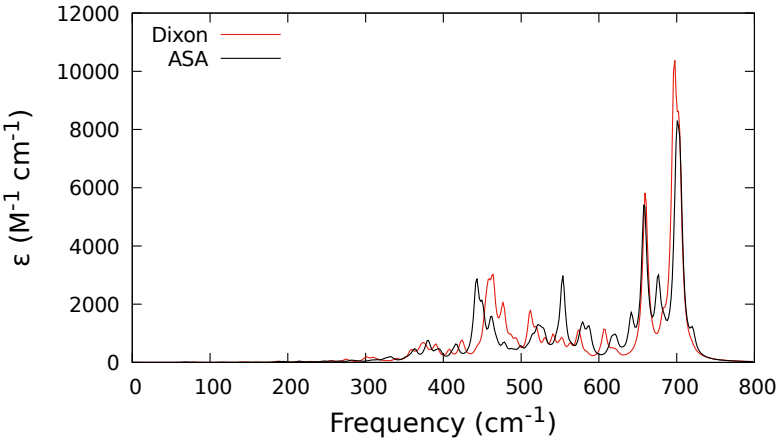

(v) $(MgO)_{27}$

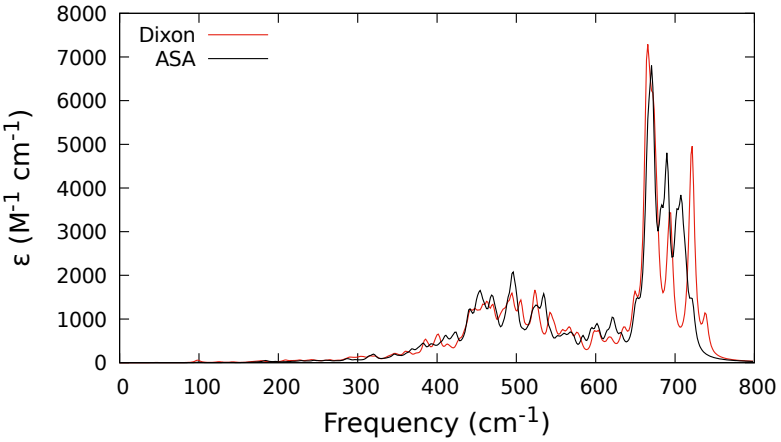

(w) $(MgO)_{28}$

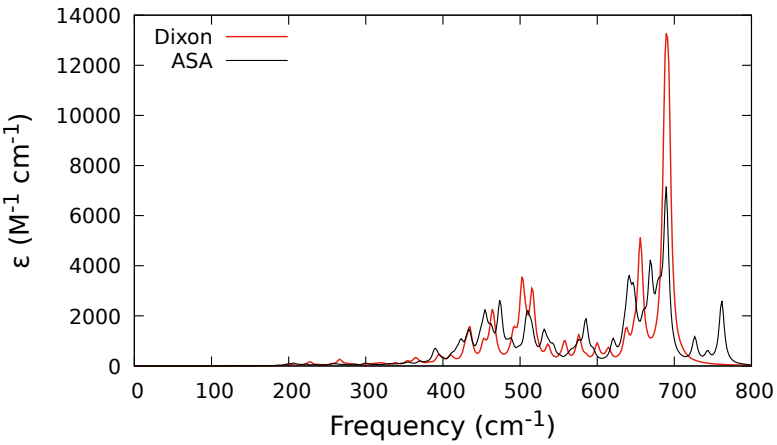

(x) $(MgO)_{29}$

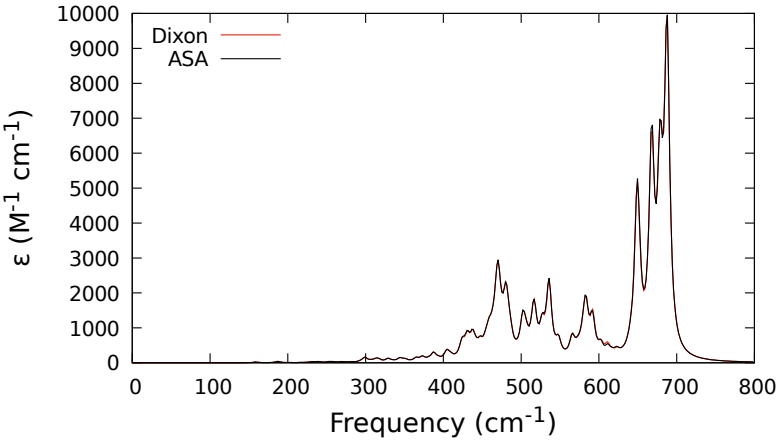

(y) $(MgO)_{30}$

Figure 11: Comparison of the IR spectra of the global minima of $(MgO)_n$ clusters obtained by Haertelt et al., Dixon et al. and the present work using ASA, followed by DFT optimisation.

Cluster	*ASA*	*DFT*	*RDF*
R	C_2	C_2	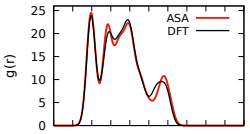
TS	C_2	C_2	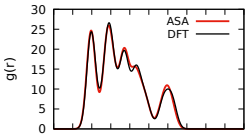
P	D_{2d}	D_{2d}	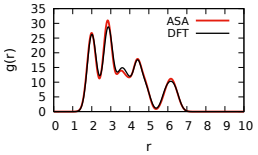

Figure 12: Comparison of ASA and DFT optimised structures for $(MgO)_8$ cluster

Cluster	*ASA*	*DFT*	*RDF*
R	D_{3h}	D_{3h}	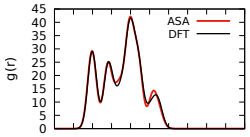
TS	C_{2v}	C_{2v}	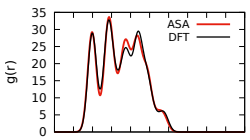
P	C_{4v}	C_{4v}	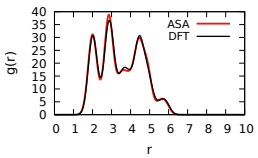

Figure 13: Comparison of ASA and DFT optimised structures for $(MgO)_9$ cluster

Cluster	*ASA*	*DFT*	*RDF*
R	 D_{3d}	 D_{3d}	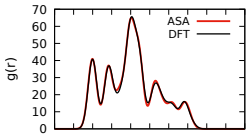
TS	 C_s	 C_s	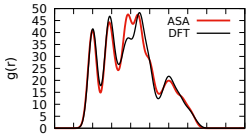
P	 C_{2h}	 C_{2h}	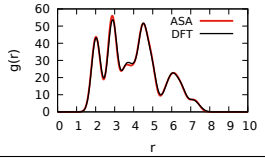

Figure 14: Comparison of ASA and DFT optimised structures for $(MgO)_{12}$ cluster

Cluster	*ASA*	*DFT*	*RDF*
R	 C_s	 C_s	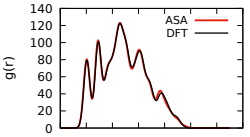
TS	 C_s	 C_s	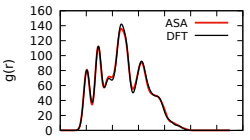
P	 C_s	 C_s	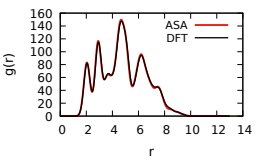

Figure 15: Comparison of ASA and DFT optimised structures for $(MgO)_{21}$ cluster